

DOI: 10.1002/ ((please add manuscript number))

Article type: Full Paper

A cast net thrown onto an interface: wrapping 3D objects with an interfacially jammed amphiphilic sheet

Mengmeng Cui, Qiang Gao, Christopher C. Bowland, Eric M. Burgeson, Kunlun Hong, Pengtao Yue, and Amit K. Naskar**

Dr. M. Cui, Dr. C. C. Bowland, Mr. E. M. Burgeson, Dr. A. K. Naskar
Carbon and Composites Group, Chemical Sciences Division, Oak Ridge National Laboratory,
Oak Ridge, TN 37831, USA
E-mail: mcui8877@gmail.com; naskarak@ornl.gov

Dr. Q. Gao, Dr. K. Hong
Center for Nanophase Materials Science, Oak Ridge National laboratory, Oak Ridge, TN
37831, USA

Prof. P. Yue
Department of Mathematics, Virginia Tech, Blacksburg, VA 24061-0123, USA

Keywords: wrapping, interfacial jamming, lignin surfactant, interfacial instability, non-equilibrium morphologies

Wrapping a three-dimensional (3D) object with a two-dimensional (2D) sheet is not uncommon, but the wrapping behavior becomes complex and interesting when the sheet is bestowed with strong interfacial activities. Amphiphilic lignin macromolecules, isolated from biomass, form a scalable thin surfactant sheet at an oil/water interface through the interfacial jamming process. The process marks three distinct stages of interfacial behavior: (a) diffusive assembly, (b) viscous assembly with retarded mobility, and (c) flexible yet irreversibly jammed rigid sheets. The surfactant sheet wraps, traps, and promptly stabilizes both oil and water droplets in non-equilibrium morphologies upon environmental stimulus. Beyond preserving exotic morphologies, the highly interfacially-active surfactant sheet also participates in morphology evolution by creating a vanishing interfacial tension and driving interfacial instability around the wrapped content, leading to novel morphologies as well as many potential applications.

1. Introduction

Wrapping 3D objects in a 2D sheet is commonly seen in nature and widely used in everyday life and industry. Protection of the encapsulated materials from the surroundings to minimize material loss or friction is the initial and the most familiar purpose of wrapping.¹ Examples include wrapping a gift in daily lives, or wrapping an electrode with a graphene sheet to accommodate volume expansion upon battery cycling.²⁻⁶ Wrapping has also been developed as a functionalization tool to endow 3D objects with desired properties, such as hydrophobicity,⁷ optical properties,^{8,9} or conductive properties.^{9,10, 11} Most recently, the range of wrapped content has expanded to liquids, with the encapsulant being either solid elastic films¹²⁻¹⁶ or solid-like jammed films of functional particles.¹⁷⁻²¹ These films are rigid enough to stabilize non-equilibrium morphologies of the wrapped liquid, thus breaking the limit of equilibrium morphologies and further creating new shapes of wrapped, encapsulated fluids with inimitable functionalities.

For traditional liquid-phase technologies, a liquid-like layer of surfactant or particles is usually used for wrapping and stabilizing liquid droplets.²²⁻²⁴ Recent studies show that sufficiently thin elastic sheets offer a novel path to spontaneously wrap liquid droplets using capillary forces, where the elastic energy of curving sheets is balanced by the reduction of interfacial energy.^{15, 16, 25, 26} Although negligible at macroscopic scales, capillary forces become dominant and are able to bend the elastic sheets when the bending rigidity of elastic sheets is vanishingly small.^{12,15, 25} The robust elastic sheets allow the liquid drops to be trapped in non-equilibrium 3D shapes via a process that is usually referred to as capillary origami.^{12, 16, 26} In previous wrapping studies, the final encapsulated 3D geometry was almost solely determined by the initial geometry of the flat thin elastic sheets, which made the process complicated and lacked versatility. The elastic sheets in previous reports were often conventional polymer thin films whose interfacial activities were too weak to manipulate the

interfacial tension and participate in morphology evolution.^{12, 15-16} A large-scale elastic sheet²⁷ with a significant interfacial activity is desired to manipulate the interface that can adapt to various non-equilibrium shapes by external influence – a stimulant for evolved morphologies at the interface.

Here, we report in-situ formation of a large-scale surfactant sheet with strong interfacial activities by interfacial jamming of poorly soluble amphiphilic lignin macromolecules in particulate form at an oil/water interface. The amphiphilic nature of the surfactant sheet enables wrapping of either water or oil droplets, while its rigidity allows it to hold the liquid phases in various non-equilibrium morphologies. The surfactant sheet is physically networked by reversible hydrogen bonding and π - π interaction, which endows it with transforming and self-healing ability. The strong interfacial activity of the surfactant sheet results in an interfacial instability, which drives evolution of interfacial morphology and novel wrapped microstructures.

2. Results and Discussion

2.1. “Soft” lignin particle surfactants

Recently, the unique properties of soft microgel particles and their function in stabilizing Pickering emulsions have attracted increasing attention.²⁸⁻³² Different from traditional rigid particles (inorganic particles), soft polymer particles preserve the rigid spherical shape in bulk solution but strongly deform, swell and flatten at an oil/water interface.³⁰⁻³² As opposed to conventional soft particles that are covalently crosslinked, this work created a new “soft particle” that is physically interconnected and prepared from a biomass-derived material – lignin^{33,34}, which further formed large-scale surfactant sheets by re-assembly and flattening at the interface. Lignin particles were prepared by gradually exchanging the solvent from acetone (a good solvent) to water (an anti-solvent)³⁵, (**Fig. 1A**)

causing the lignin chains to collapse and aggregate into particles due to a loss of solubility. A homogenous dispersion was obtained with uniform particles in a diameter around 500 nm (**Fig. 1B**). Owing to lignin's hydrophobic aromatic backbone and hydrophilic functional groups,^{33, 36} i.e. hydroxyls, carboxyls, and aldehydes, the lignin particles exhibited a strong interfacial activity that drives them to self-assemble at a toluene/water interface.³⁷ This resulted in a stable emulsion of lignin particles that was stable for over one month as observed under optical microscopy (**Fig. 1C**). The strong interfacial activity was proved by the dynamic interfacial tension measurement at the water/toluene interface (**Fig 1D**), in which the interfacial tension decreased from 38 mN/m to 17 mN/m.

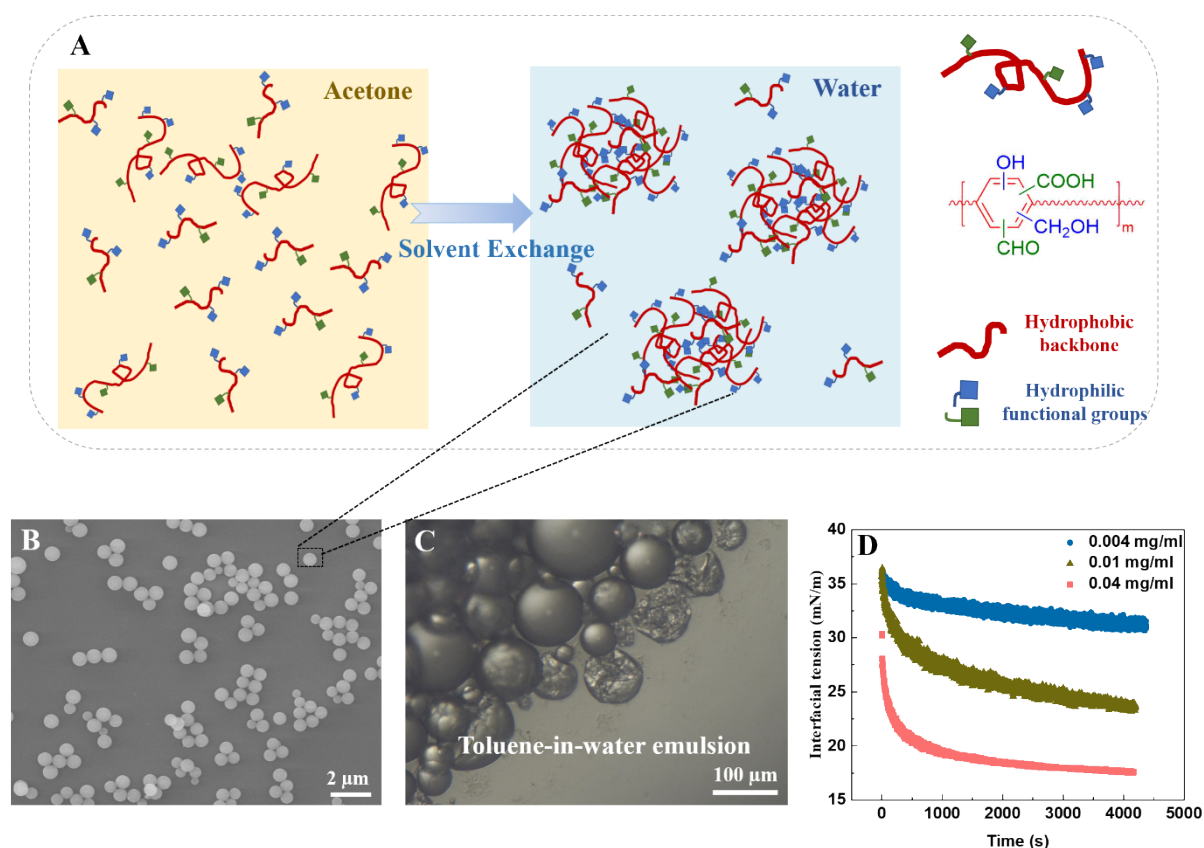


Fig.1 Preparation and interfacial activity of “soft” lignin particle surfactants. (A) Lignin particle preparation via solvent exchange. The lignin polymers bearing multi-functional groups around an aromatic backbone gradually lose solubility and form a homogeneous suspension when the water content slowly increases in solvent. (B) SEM observation of uniform lignin particles with ~500 nm diameter. (C) Optical image of a toluene-in-water emulsion stabilized by lignin particles. (D) Dependence of the dynamic interfacial tension of water/toluene on the concentration of lignin particles. The strong interfacial activity of particles comes from the hydrophobic backbone and the hydrophilic functional groups in the lignin chemical structure.

2.2. In-situ formation of large-scale surfactant sheet

The huge number of functional groups that are capable of forming hydrogen bonding lead to the strong self-association and physical crosslinking inside of the particles. However, upon contact with the interface, the lignin particles were deformed and flattened, and formed a 2D surfactant sheet with an extreme aspect ratio (**Fig. 2A**; **Fig. S1**, see supporting information). Different from conventional soft particles whose deformations were limited by particle elasticity due to covalent crosslinking,³⁰⁻³² the lignin particles were completely spread out at the interface in the presence of weak crosslinking, i.e. hydrogen bonding. The driving force of spreading came from the reduction in interfacial energy by maximizing the surfactant covered area and decreasing the unfavorable contacts between oil and water. The oil/water systems were designed so that lignin had very limited solubility in both water and oil phases, e.g. toluene or dichloromethane³⁸, which resulted in spreading instead of detaching of particles from the interface to the bulk solution. This phenomenon largely enhanced the efficiency of lignin particles' interfacial activity. As shown in **Fig. 1D**, the interfacial tension decreased by about 17 mN/m at a low concentration of lignin particles (0.04 mg/ml) after 10 min of surface age.

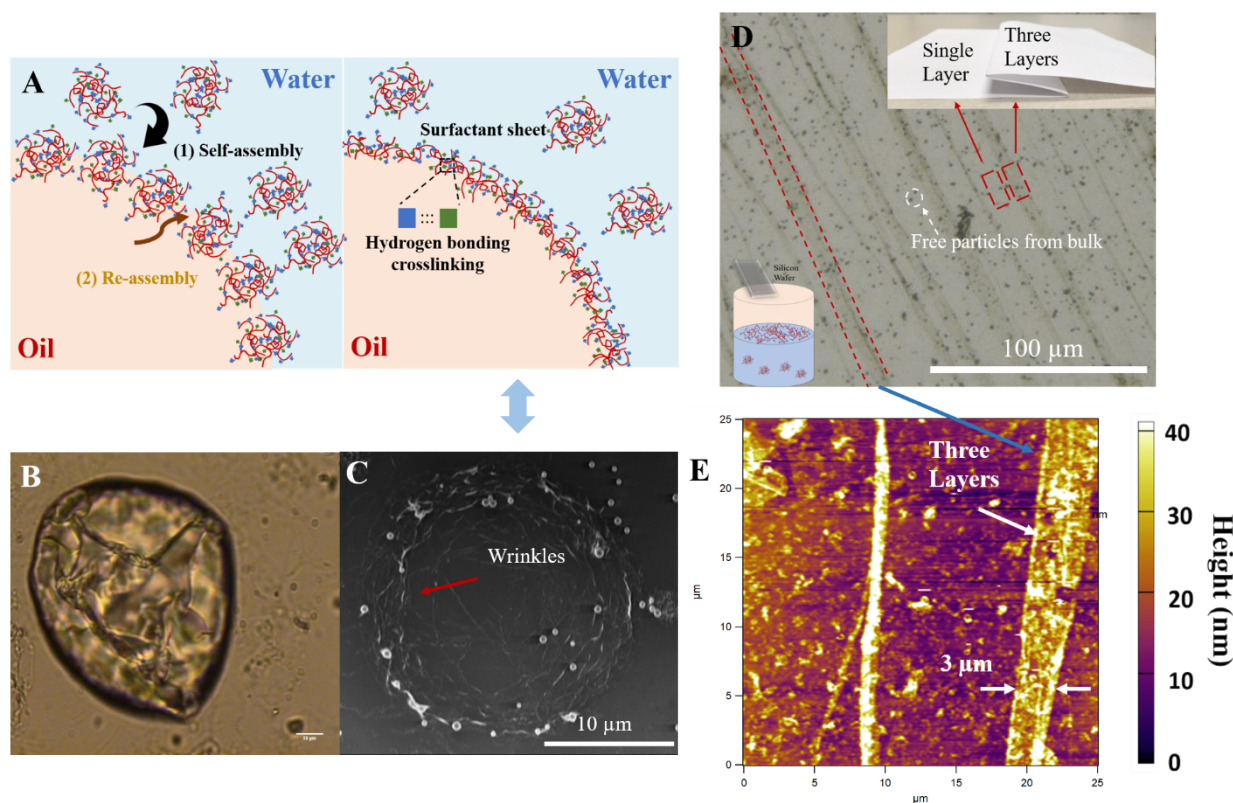


Fig.2 Large-scale surfactant sheet. (A) Schematic illustration of the formation of the surfactant sheet: amphiphilic lignin particles first self-assemble at the interface; upon contact with the oil phase, particles deformed and unfolded at the interface to maximize the coverage and to decrease the unfavorable interactions between immiscible liquids. (B) Optical microscopy observed the buckling of a partially dried emulsion droplet, which proves a solid-like interface. (C) Another evidence of a solid-like interface is provided by the SEM image of a thin film with a few wrinkles. The wrinkles are a result of the collapse of an emulsion droplet after solvent evaporation. (D) Preparation of a large-scale surfactant sheet by floating a thin surfactant film on a silicon wafer at a planar interface. Following the folding pattern in the inset, tri-layer wrinkles (circled in red) appear on the thin film during the floating process, accompanied with free lignin particles (circled in white) from the aqueous phase. (E) AFM image of a thin film with a tri-layer wrinkle, prepared according to Fig.2 (D). The thickness of the thin film is calculated by dividing the measured height of wrinkle by two.

Buckling was observed on the surface of a partially dried emulsion droplet under the optical microscope, indicating a solid-like interface (**Fig. 2B**). According to previous reports¹⁷⁻¹⁹, such surfactant films at the interface were often a collection of jammed particles. If that was the case, the lignin surfactant film in this work would have a rough surface because of the aggregation of particles. However, in the SEM image of a dried emulsion droplet (**Fig. 2C**), the solid-like film lacked the expected roughness, and only a few crumpled geometries, like wrinkles, occurred occasionally.

Another unexpected discovery was the thickness of a floating film at the toluene/water interface. Because of the minimal elastic modulus, the thin film was easily bent or folded during the floating process. When the film was folded like the paper as shown in the **Fig. 2D** inset, a wrinkle that has three layers of film would appear (see schematic in **Fig. S1D**). In the meantime, because the substrate inevitably contacted free lignin particles from water during the floating process, the collected film always exhibited surface deposited particles of half micron diameters.

By measuring the height of the tri-layer wrinkles under atomic force microscopy (AFM), we were able to calculate the thickness of one single layer of the thin film (**Fig. 2E**). If it was an interfacially jammed particle film, the thickness would be comparable to the particle diameter, i.e. 500 nm. However, based on the AFM measurement, the thickness of a floating film was only about several nm. This once again proved that the lignin surfactant films were not simply particles. Instead, the lignin particles deformed, flattened into thin sheets, and spread out at the interface, just like a thrown-out cast net.

2.3. Jamming transition

The surfactant sheet is essentially formed through an interfacial jamming process, during which the packing density³⁹ gradually increases until the interface reaches a solid-like state. Therefore, understanding the jamming process will help us understand the formation mechanism of lignin surfactant sheets. The jamming transition can be accelerated by abruptly increasing the packing density. As shown in **Fig. 3A**, an abrupt withdrawal of interior fluid from the droplet led to a sudden decrease of interfacial tension, due to the increase of packing density. Since the system has already reached an equilibrium state, the total number of particles at the interface is fixed. Therefore, when the interfacial area is decreased, the particle packing density rises, which reduces the interfacial tension. On the other hand, measuring the recovery of interfacial tension after each droplet retraction probes the evolution of interfacial

viscoelastic properties over the course of a jamming transition. In Fig. 3A, three types of interfacial tension recovery were identified, marking three different stages of interfacial restructuring during the formation of the lignin 2D sheet.

In the first stage, no wrinkles were formed at the interface after the droplet retraction, as the interface was not able to support the applied stress, and the applied stresses were spatially uniform. The interfacial tension recovered relatively fast, as compared with the next stage. This indicated a liquid-like diffusive state of particles at the interface in this stage. When the packing density was further increased and reached stage II, the recovery of interfacial tension slowed down after the droplet retraction because the particle assembly transitioned to a viscous state from the previous liquid-like diffusive state. The wrinkles first appeared upon droplet retraction as the interface was subjected to a large compression in the latitudinal direction⁴⁰⁻⁴³ but then disappeared within 4 seconds (**Supporting Movie 1**). Applying another droplet retraction in late stage II resulted in an even slower recovery of interfacial tension, and the lifetime of wrinkles extended to beyond 90 seconds (**Fig. 3C**). At this stage, the packing density increased, and the interface layer became more networked and more viscoelastic, accompanied by a gradual loss of fluidity. Stage II was a transition stage during which the interface was developing its solid-like properties. Further increasing the packing density eventually led to the final stage III. The interfacial tension did not recover after the droplet retraction and the wrinkles on the surface persisted. The non-equilibrium shape of the partially retracted droplet was held by the rigidity of interface when the interface became a solid-like film in stage III (**Supporting Movie 3**).

In many previously reported interfacial systems, the recovery of interfacial tension, as well as the fading of wrinkles, would occur when the packing density passed a threshold of glassy interface formation, such that the interface relaxes to an equilibrium state by desorption of surfactant particles.^{44, 45} In this lignin-based system, however, several pieces of evidence

suggested a different mechanism. First, when the packing density was far from the threshold in stage I, the recovery of interfacial tension still appeared. Secondly, in stage III, a plateau, instead of a recovery, of interfacial tension appeared right after the droplet retraction. This indicated that desorption of lignin particles during the droplet retraction was negligible. Thirdly, the equilibrium interfacial tension after recovery was always lower than the initial interfacial tension before droplet retraction, regardless of the stage (**Fig. 3A, Fig. S2B**). This suggested that after each retraction, the packing density always increased.

Further evidence proving the nonexistence of interfacial desorption is the relationship between dynamic interfacial tension and surface area after each droplet retraction. The interfacial tension at a time t would be $\gamma(t) = \gamma_{oil/water} - k\Gamma_t A_t$, where Γ_t is the packing density, A_t is the interfacial area, and k is a constant denoting the interfacial drop caused by an individual lignin particle. If no desorption occurred during the retraction and recovery, the total mass of lignin at the interface would stay the same, i.e. $\Gamma_0 A_0 = \Gamma_t A_t$, where Γ_0 and A_0 are respectively packing density and interfacial area when wrinkles began to form. And the previous equation can be written as:

$$\gamma(t) = \gamma_{oil/water} - k\Gamma_0 \frac{A_0}{A(t)} \quad (1)$$

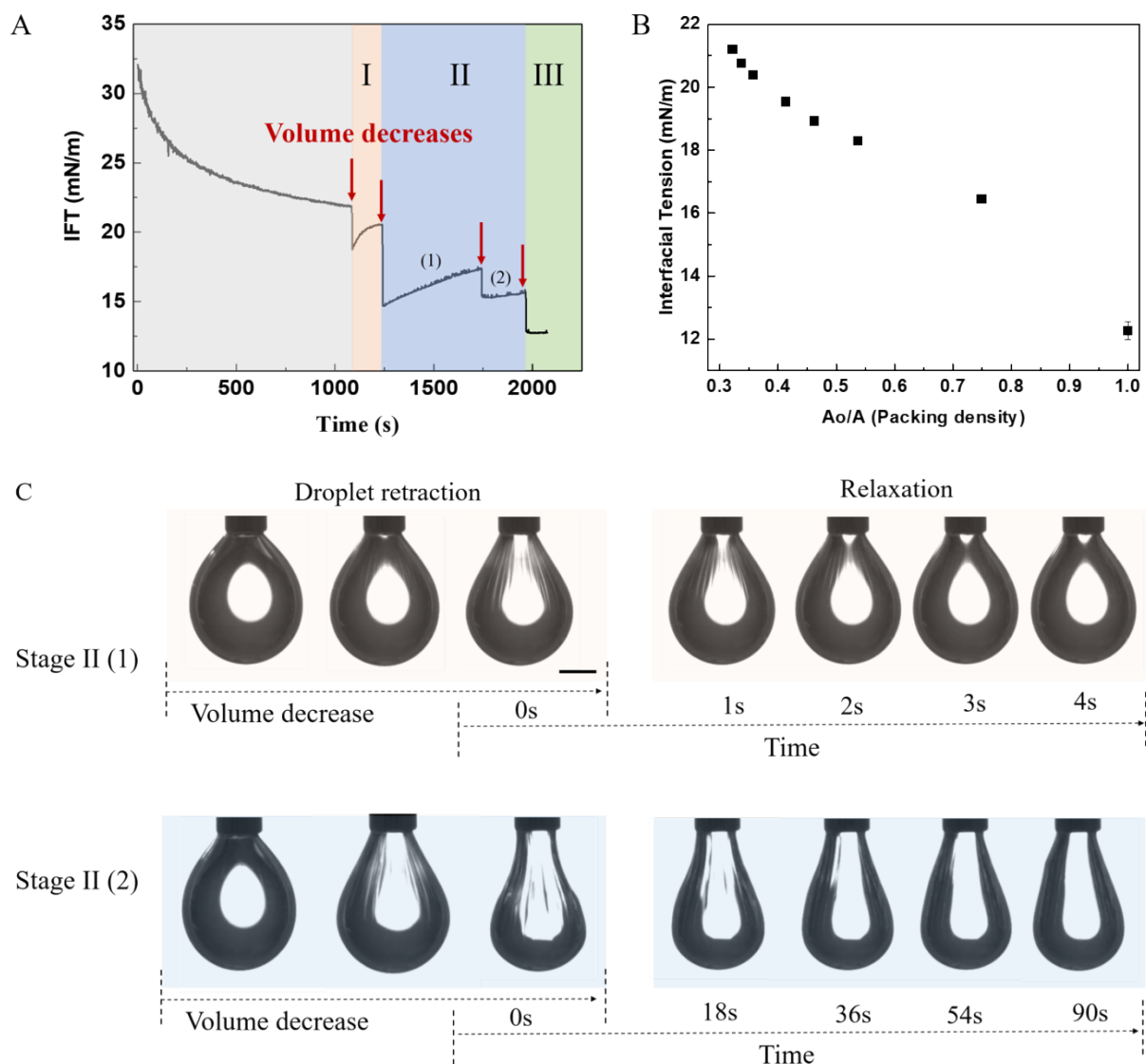


Fig.3 (A) Evolution of the toluene/water interfacial tension $\gamma(t)$ measured by the pendant drop method after sudden increase of lignin particle packing density, which resulted from the droplet volume decreases. (B) The approximate linear dependence of interfacial tension on the area strain, A_0/A . Both the equilibrium interfacial tension (y axis) and surface area (A) are obtained after retraction, while A_0 is when wrinkles begin to form. (C) The droplet recovery after retraction in stage II is dependent on the viscoelastic property of surfactant sheet.

To verify the validity of Equation 1, a droplet was consecutively retracted in stage II. After each retraction, the interfacial tension and the surface area at the new equilibrium/steady state (i.e. when the droplet fully recovered) were measured. The plot of interfacial tension $\gamma(t)$ against A_0/A_t was indeed linear (Fig. 3B), just as what Equation 1 predicted. Thus, the

hypothesis of negligible desorption is valid, and the interfacial tension recovery was not caused by the desorption of particles.

So, what was contributing to the interfacial tension recovery? We believe that it came from the reorganization of particles at the interface. When the droplet volume was reduced, the droplet was stretched in the vertical direction and the Laplace pressure at the upper part of the droplet was reduced, leading to the inward collapse of the droplet (**Fig. S3**). Thus, in addition to the stretching in the vertical direction, the upper droplet surface also experienced a compression in the latitudinal direction. This caused a local increase in particle concentration as compared with the lower part of the droplet surface. After volume reduction, the particles reorganized and finally approached a uniform concentration on the droplet surface. At a low packing density (before the jamming formed), the droplet surface was still fluid-like and the reorganization process was very short because of the Marangoni flow. After the jamming transition, the interface became more solid-like, which prolonged the reorganization process. As shown in **Fig. S2B**, the recovery lasts for over two hours for the interface with a high packing density. If desired, functionalities in the oligomers can be tailored to devise rapid and irreversible jamming via chemical crosslinking between the adjacent molecules. In such cases, however, shape recovery or restructuring may not be possible within any given experimental time.

2.4. Reconfigurable wrapping of a droplet in non-equilibrium morphologies

Not only could the surfactant sheet stably wrap either water or oil droplet in their immiscible liquid, but it was also able to promptly repair itself upon breakage and reconfigure the wrapped geometry. This was exemplified by a suction-and-injection experiment of a wrapped water droplet in toluene. As shown in image series **Fig. 4**, when a part of a water droplet was retracted, some toluene around the retracted water and the surfactant sheet at the

interface were also withdrawn into the needle. Inside the constrained space in the needle, the surfactant sheet temporarily reassembled at the new cylindrical interface (**Supporting Movie 2**). Further withdrawing through the syringe created a large shear force and tore apart the once continuous toluene/water interface, as well as the surfactant sheet, into smaller pieces. These small pieces of surfactant sheets then wrapped either water or toluene nearby into non-equilibrium morphologies in the needle. When the same volume of retracted liquid was refilled into a droplet from the needle, two transformed droplets appeared: an irregularly shaped toluene droplet was contained inside of a cylindrical water droplet. Complete refilling of the droplet brought back the spherical shape which, however, contained a toluene phase wrapped by surfactant sheet. These extraordinary shapes were the evidence of the quick reassembly and reconfiguration capability of the surfactant sheets.

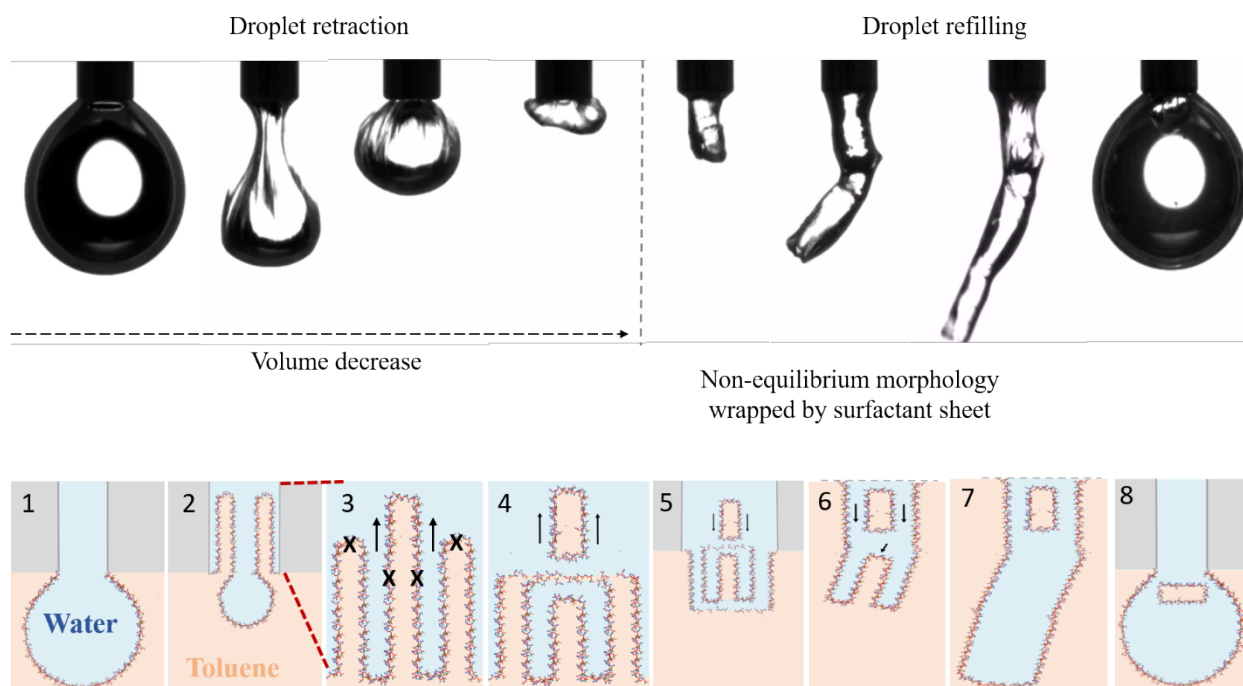


Fig. 4 The creation of a non-equilibrium morphology, i.e. a cylindrical water droplet containing a toluene droplet inside, by suction-and-injection of a droplet wrapped by surfactant sheets. The formation of the cylindrical water droplet inside the needle and the formation of the contained toluene droplet by shear failure of the surfactant sheet are illustrated in the bottom row of the scheme.

Here, the wrapping of the irregular shaped toluene droplet was similar to an observation in a previous study, where for a fixed area, an ultrathin sheet automatically achieved optimally efficient shapes that maximized the enclosed volume of liquid.¹⁵ However, the surfactant sheets in this report were crosslinked by dynamic hydrogen bonding, which prevented the cleaved surfactant sheets from falling apart, and allowed them to either reconnect with each other or to form new individual wraps at new interfaces. This is how the cylindrical water droplet was formed. Despite the relatively weak strength of hydrogen bonding, the surfactant sheet could resist certain stress and keep the pre-restricted non-equilibrium shape, partially owing to the high Young's modulus of lignin. As shown in Movie 3, the non-equilibrium shape was trapped until further filling. Therefore, when the retracted water was injected back through the needle, the wrapped toluene droplet kept floating at the top of the growing cylindrical water droplet.

2.5. Wrapped porous microparticles: morphology transition induced by surfactant sheet

Interfacial instability is a contemporary topic that is extensively studied in polymer science to develop novel morphologies,⁴⁶⁻⁵⁰ with one examples being hierarchically structured microparticles during solvent removal from oil-in-water emulsions.⁴⁷⁻⁴⁹ The fundamental principle is that the interface is full of fluctuations and the undulation amplitude is controlled by the interfacial tension. A reduction in interfacial tension enhances undulation amplitude, and various microstructures can form at the interface transiently when the undulation amplitude is significant enough. The surfactant sheet features strong interfacial activity. Therefore, it not only wraps the liquid droplet, just like the conventional thin elastic sheet does, but also assists in the morphological transition of the droplet interface.

Here, a dichloromethane/water emulsion with 10 mg/ml of PS_{38k}-PEO_{11k} copolymers dispersed in aqueous phase was selected as a model system to demonstrate the efficacy of the

surfactant sheet. In the native system without the lignin particles, budded and fused vesicles were formed on the surface of microparticles after solvent removal (**Fig. 5A, B**), which is resulted from the surface undulation. However, when lignin particles were present in the aqueous phase, a porous structure sealed under a membrane would form after solvent was removed (**Fig. 5C, D, E**). The significant morphology difference was a result of the differently levels of interfacial tension reduction, depending on the species and behaviors of the surfactant at the interface. When there was only amphiphilic block-copolymers in the system (**Fig. 5A**), the interfacial tension was decreased, but not to a low enough value for a spontaneous emulsification. The weak undulation of the interface only resulted in some fine structures on the surface of dried droplet. On the other hand, when both the copolymer and the lignin particles adsorbed at the interface, the interfacial tension was decreased enough to achieve spontaneous emulsification. Moreover, as the lignin surfactant sheet expanded at the interface and gradually formed a jammed state, the interfacial tension was further reduced and the interface was destabilized as well, both of which drove the morphology transition. During the spontaneous emulsification, many water droplets were formed inside the preliminary oil droplet, forming a system of water/oil/water double emulsions. Thus, a hierarchically porous structure appeared after the solvent was evaporated. The formation mechanism of such sealed porous structure is explained in **Fig. 5F**.

Interestingly, this hierarchically sealed porous morphology was also a result of the solid-like thin sheet at the interface. While the interfacial jamming strengthened the interface instability, the interface was also becoming more and more solid-like during the morphology transition. Were the surfactants mobile at the interface, open-porous structures would have appeared after solvent removal.⁵¹⁻⁵² The capability of in situ trapping the morphology evolution is one of the novelties of this lignin system.

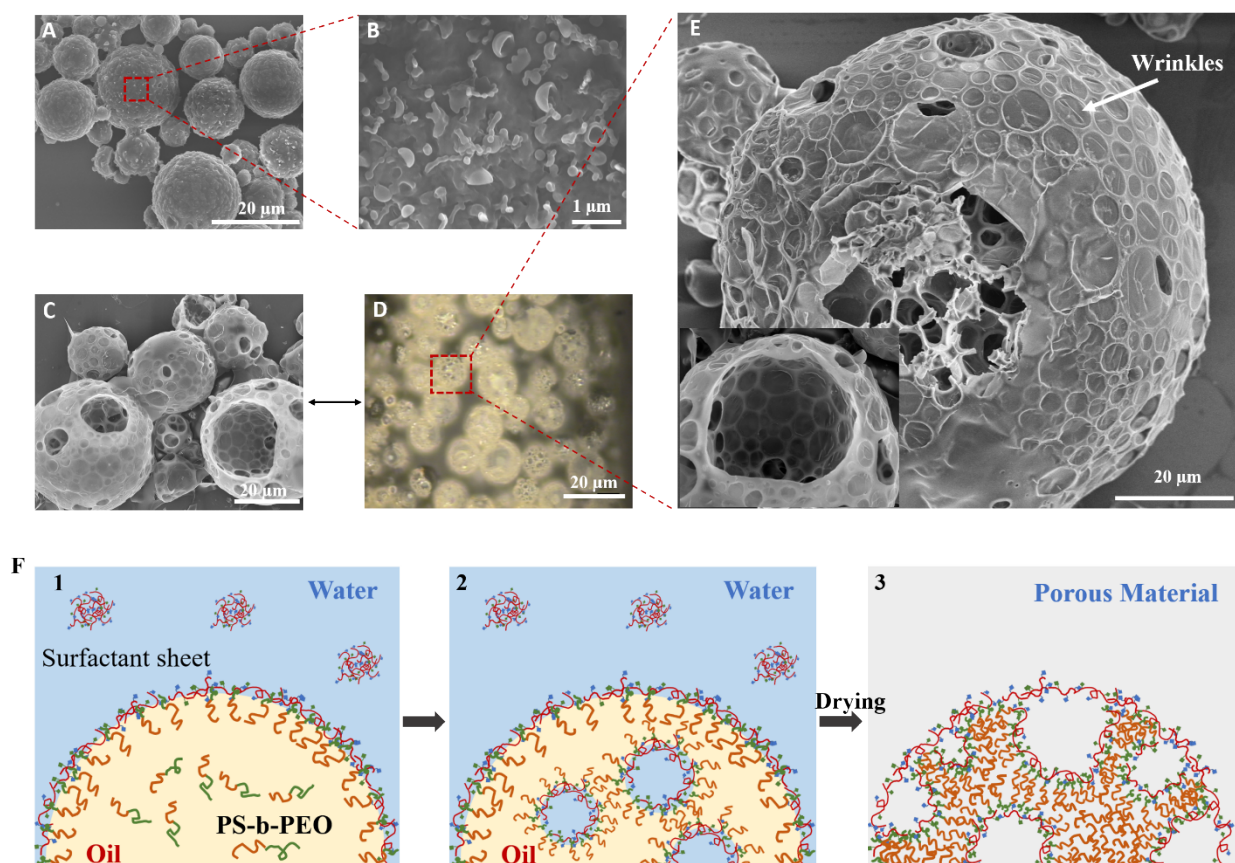


Fig. 5 (A) SEM image of PS_{38k}-PEO_{11k} microparticles formed by removal of dichloromethane from emulsion droplets. (B) SEM image of fused budding vesicle on the surface of microparticles formed in A. (C) SEM image of lignin surfactant sheet wrapped PS_{38k}-PEO_{11k} porous microparticles. (D) Optical micrographs in transmission mode showing the porous structure inside microparticles. (E) SEM image of partly peeled-off microparticles showing that some pores inside of microparticles are also covered by the surfactant sheet. It also shows there is some buckling of the thin sheet. (F) Schematic illustration of the formation of the hierarchically wrapped porous microparticles. The surfactant sheet and PS_{38k}-PEO_{11k} self-assemble at the interface and synergistically reduce the interfacial tension, further inducing interfacial instability.

The surfactant sheet not only allowed the solvent to permeate and evaporate, but also remained stable during this process due to its solid-like property, essentially working as a membrane. Underneath the exterior membrane that wrapped around a microparticle, the pores inside the microparticle were also similarly covered by a membrane, indicating a hierarchical structure. Additionally, buckled small-scale structures were also found on the microparticle surface during the shrinking. The existence of membranes inside the microparticles and the

buckling on the surface proved that a solid-like sheet was pre-formed at the interface before the solvent removal. Thus, aided by the surfactant sheet, a new morphology of hierarchically wrapped porous microparticles was created by interfacial roughening.

3. Conclusion

We developed a scalable and efficient method to prepare large-area surfactant sheets by unfolding lignin particles into a thin sheet at the oil/water interface, like a cast net thrown onto an interface. These thin sheets were then dynamically crosslinked by hydrogen bonding during an interfacial jamming process consisting of three different stages. Due to the amphiphilicity of lignin, these thin sheets were highly active at interfaces and could wrap droplets into non-equilibrium morphologies. Its capability of prompt reassembly at the interface also enabled easy formation of novel shapes as well as a “memory” of the shapes. Moreover, due to its significant interfacial activity, the surfactant could create novel non-equilibrium morphologies. The large-scale surfactant sheet not only leads to many potential applications, with one example being the sealed porous microparticles that were hierarchically covered by membranes, but also provides a new encapsulant material to study the wrapping behavior and interfacial jamming process.

4. Experimental Section

Preparation of lignin particles: Spherical lignin nanoparticles were prepared by dialysis, during which the once solubilized lignin aggregated into particles due to the progressive loss of solubility. The softwood Kraft-treated lignin was provided by Kruger Wayagamack Inc. The lignin was first dissolved in acetone at a concentration of 10 mg/ml. Subsequently, the solution was filtered through a 0.45 μm syringe filter and transferred into a dialysis bag which was made of regenerated cellulose (Fisher brand, #21-152-14). The dialysis bag was

immersed into deionized water for 72 hrs. Then, the lignin particle dispersion was retrieved from the dialysis bag and centrifuged at 2000 rpm for 5 min, and the supernatant was retrieved for the following experimentation. To understand the size and morphology of the particles, the particle dispersion was dried on a silicon wafer and prepared for morphology characterization by scanning electron microscope (SEM) (Hitachi S4800). The concentrations of lignin aqueous solution were obtained by thermogravimetric analysis (TGA) that provided the weight of lignin nanoparticle after water evaporation.

Emulsion preparation: The emulsions were prepared by shaking an oil/water mixture with a volume ratio of 1:9. The water phase contained 0.04 mg/ml lignin nanoparticles while the oil phase was toluene. The oil droplets dispersed in water were first characterized under an optical microscope. Then the emulsions were drop cast on a silicon wafer and dried overnight to remove the solvent. The morphologies of dried droplets were characterized by SEM.

Thickness measurement by Atomic Force Microscope (AFM): The large-scale surfactant sheet was prepared by carefully adding toluene at the top of water phase, which contains 0.04 mg/ml lignin nanoparticles, in a vial. The vial was left still in a hood for 48 hrs. An obvious interface was formed between water and toluene where the lignin nanoparticles self-assembled and formed the surfactant sheet. Then the surfactant sheet was collected by floating the film on a silicon wafer by inserting the silicon wafer into the vial, during which wrinkles were formed on the film. This surfactant sheet was characterized by optical microscopy and AFM. AFM images were recorded with a Cypher AFM microscope from Asylum Research (Oxford Instruments), operating in the tapping mode in air using cantilevers with a spring constant of 30 N m^{-1} (Bruker, MPP-11100-10).

Interfacial tension measurement: The dynamic interfacial tension was measured by a pendant geometry in a tensiometer (Kruss DSA30s). A pendant droplet containing an aqueous dispersion of lignin particles was suspended in a continuous phase of toluene. The evolution of droplet shape with time was recorded by a camera and fitted by Young-Laplace equation to determine the dynamic interfacial tension.

Jamming transition reflected by interfacial tension recovery: At the beginning, a pendant drop containing an aqueous dispersion of lignin particles was created and suspended from a syringe needle in toluene. And the syringe was fixed on a tensiometer which provided the automatic injection & suction, as well as the capability of measuring the interfacial tension at the oil/water interface. A decrease of droplet volume was made by withdrawing some liquid into the syringe, which resulted in a decrease of surface area at the same time. When the lignin nanoparticles self-assembled at the interface and reached the equilibrium state, the number of nanoparticles at the interface remains constant. So, a sudden decrease of interfacial tension was observed as a result of nanoparticle number increase during suction.

The suction-and-injection experiment: The cyclic suction-injection experiment was conducted as described in the main text by removing and injecting liquid inside the droplet. A camera connected to the computer recorded the behavior and morphology change of droplet.

Preparation of sealed porous microparticles: The porous microparticles were made from droplets in emulsion. The emulsion was prepared as described in the main text. The oil droplets were from a dichloromethane solution with 10 mg/ml PS_{38k}-b-PEO_{11k} copolymer (purchased from Polymer Source). Meanwhile, the continuous phase contained 0.04 mg/ml lignin nanoparticle surfactant that stabilized the emulsions by reducing the interfacial tension and forming physical steric hindrance against coalescence. The porous microparticles were

obtained by solvent evaporation of droplets on a glass coverslip open to air at room temperature. During the evaporation, morphology evolution occurred due to interfacial instability which further came from the low interfacial tension. Depending on the geometry of the container and the quantity of emulsion, the evaporation of solvent would take tens of minutes to hours. The dried droplets were characterized by SEM.

Supporting Information

Supporting Information is available from the Wiley Online Library or from the author. Additional characterization data (PDF); Movie of relaxation of jammed thin film (mp4); Movie of reconfigurable wrapping of droplet in non-equilibrium morphologies (mp4); Movie of non-equilibrium morphology's stability (mp4)

Acknowledgements

This research at Oak Ridge National Laboratory, managed by UT Battelle, LLC, for the U.S. Department of Energy (DOE) under contract DE-AC05-00OR22725, was sponsored by the Office of Energy Efficiency and Renewable Energy Bioenergy Technologies Office Program. Q. Gao was supported as part of the Fluid Interface Reactions, Structures and Transport (FIRST) Center, an Energy Frontier Research Center funded by the U.S. Department of Energy, Office of Science, Office of Basic Energy Sciences. AFM and Interfacial tension measurements were conducted at the Center for Nanophase Materials Sciences, which are DOE Office of Science User Facility.

This manuscript has been authored in part by UT-Battelle, LLC, under contract DE-AC0500OR22725 with the US Department of Energy (DOE). The US government retains and the publisher, by accepting the article for publication, acknowledges that the US government retains a nonexclusive, paid-up, irrevocable, worldwide license to publish or reproduce the published form of this manuscript, or allow others to do so, for US government purpose. DOE will provide public access to these results of federally sponsored research in accordance with the DOE Public Access Plan (<http://energy.gov/downloads/doe-public-access-plan>).

Author contributions: M.C. and A.K.N. conceived the idea and designed the project; M.C., Q.G., C.C.B., E.M.B., K.H., and P.Y. conducted the experiments; M.C. and A.K.N. analyzed the data; M.C. and A.K.N. drafted the manuscript.

Received: ((will be filled in by the editorial staff))

Revised: ((will be filled in by the editorial staff))

Published online: ((will be filled in by the editorial staff))

References

- [1] J. D. Paulsen, *Annu. Rev. Conden. Matter P.* **2019**, 10, 431-450.
- [2] D. Berman, S. A. Deshmukh, S. K. R. S. Sankaranarayanan, A. Erdemir, A. V. Sumant, *Science* **2015**, 348, 1118-1122.
- [3] H. Wang, Y. Yang, Y. Liang, J. T. Robinson, Y. Li, A. Jackson, Y. Cui, H. Dai, *Nano Lett.* **2011**, 11, 2644-2647.

- [4] J. Luo, X. Zhao, J. Wu, H. D. Jang, H. H. Kung, J. Huang, *J Phys Chem Lett* **2012**, 3, 1824-1829.
- [5] L. H. Hu, F. Y. Wu, C. T. Lin, A. N. Khlobystov, L. J. Li, *Nat Commun* **2013**, 4.
- [6] L. N. Chong, X. Q. Zeng, W. J. Ding, D. J. Liu, J. X. Zou, *Adv Mater* **2015**, 27, 5070.
- [7] J. Ge, L. A. Shi, Y. C. Wang, H. Y. Zhao, H. B. Yao, Y. B. Zhu, Y. Zhang, H. W. Zhu, H. A. Wu, S. H. Yu, *Nat Nanotechnol* **2017**, 12, 434-440.
- [8] H. Fuchs, H. Ohst, W. Prass, *Advanced Materials* **1991**, 3, 10-18.
- [9] X. Zhu, Z. Ge, S. Wu, *Journal of Display Technology* **2006**, 2, 1-20.
- [10] B. LeBorgne, S. Liu, X. Morvan, S. Crand, R. A. Sporea, N. Lu, M. Harnois, *Advanced Materials Technologies* **2019**, 1800600.
- [11] M. L. Hammock, A. Chortos, B. C.-K. Tee, J. B-H. Tok, Z. Bao, *Adv. Mater.* **2013**, 25, 5997.
- [12] C. Py, P. Reverdy, L. Doppler, J. Bico, B. Roman, C. N. Baroud, *Phys. Rev. Lett.* **2007**, 98, 156103.
- [13] L. C. Gao, T. J. McCarthy, *Langmuir* **2008**, 24, 9183-9188.
- [14] G. McHale, *Langmuir* **2009**, 25, 7185-7187.
- [15] J. D Paulsen, V. Démery, C. D. Santangelo, T. P. Russell, B. Davidovitch, N. Menon, *Nat Mater* **2015**, 14, 1206-1209.
- [16] D. Kumar, J. D. Paulsen, T. P. Russell, N. Menon, *Science* **2018**, 359, 775-778.
- [17] S. U. Pickering, *J. Chem. Soc., Trans.* **1907**, 91, 2001-2021.
- [18] A. D. Dinsmore, M. F. Hsu, M. G. Nikolaides, M. Marquez, A. R. Bausch, D. A. Weitz, *Science* **2002**, 298, 1006.
- [19] Y. Lin, H. Skaff, T. Emrick, A. D. Dinsmore, T. P. Russell, *Science* **2003**, 299, 226-229.
- [20] M. Cui, T. Emrick, T. P. Russell, *Science* **2013**, 342, 460-463.
- [21] M. Cui, C. Miesch, I. Kosif, H. Nie, P. Y. Kim, H. Kim, T. Emrick, T. P. Russell, *Nano Lett* **2017**, 17, 6855-6862.
- [22] R. Aveyard, B. P. Binks, J. H. Clint, *Adv. Colloid Interface Sci.* **2003**, 100, 503-546.
- [23] Y. Chevalier, M. Bolzinger, *Colloids Surf. A* **2013**, 439, 23-34.
- [24] G. McHale, M. I. Newton, *Soft Mater* **2015**, 11(13), 2530-2546.
- [25] B. Roman, J. Bico, *J. Phys.: Condens. Matter* **2010**, 22, 493101.
- [26] A. Antkowiak, B. Audoly, C. Jossierand, S. Neukirch, M. Rivetti, *P Natl Acad Sci USA* **2011**, 108, 10400-10404.
- [27] J. Kim, L. J. Cote, F. Kim, W. Yuan, K. R. Shull, J. Huang, *J Am Chem Soc* **2010**, 132, 8180-8186.
- [28] W. Richtering, *Langmuir* **2012**, 28, 17218-17229.
- [29] J. Li, Y. Hu, J. J. Vlassak, Z. Suo, *Soft Matter* **2012**, 8, 8121.
- [30] A. M. Rumyantsev, R. A. Gumerov, I. I. Potemkin, *Soft Matter* **2016**, 12, 6799.
- [31] M. Kwok, G. Sun, T. Ngai, *Langmuir* **2019**, 35, 4205-4217.
- [32] F. Camerin, M. A. Fernandez-Rodriguez, L. Rovigatti, M. Antonopoulou, N. Gnan, A. Ninarello, L. Isa, E. Zaccarelli. *ACS Nano* **2019**, 13, 4548-4559.
- [33] A. J. Ragauskas, G. T. Beckham, M. J. Bidy, R. Chandra, F. Chen, M. F. Davis, B. H. Davison, R. A. Dixon, P. Gilna, M. Keller, P. Langan, A. K. Naskar, J. N. Saddler, T. J. Tschaplinski, G. A. Tuskan, C. E. Wyman. *Science* **2014**, 344 (6185), 1246843.
- [34] R. Rinaldi, R. Jastrzebski, M. T. Clough, J. Ralph, M. Kennema, P. C. A. Bruijninx, B. M. Weckhuysen, *Angew. Chem. Int. Ed.* **2016**, 55, 8164-8215.
- [35] Y. Qian, Y. Deng, X. Qiu, H. Li, D. Yang, *Green Chem.* **2014**, 16, 2156.
- [36] M. Cui, N. A. Nguyen, P. V. Bonnesen, D. Uhrig, J. K. Keum, A. K. Naskar, *ACS Macro Lett.* **2018**, 7(11), 1328-1332.
- [37] M. Ago, S. Huan, M. Borgher, J. Raula, E. I. Kauppinen, O. J. Rojas, *ACS Appl. Mater. Interfaces* **2016**, 8, 23302-23310.

- [38] J. Sameni, S. Krigstin, M. Sain, *BioResources* **2017**, 12(1), 1548-1565.
- [39] A. J. Liu, S. R. Nagel, *Nature* **1998**, 396, 21-22.
- [40] D. Carvajal, E. J. Laprade, K. J. Henderson, K. R. Shull, *Soft Matter* **2011**, **7**, 10508-10519.
- [41] B. Madivala, J. Fransaer, J. Vermant, *Langmuir* **2009**, **25**, 2718-2728.
- [42] S. Knoche, D. Vella, E. Aumaitre, P. Degen, H. Rehage, P. Cicuta, J. Kierfeld, *Langmuir* **2013**, **29**, 12463-12471.
- [43] P. Erni, H. A. Jerri, K. Wong, A. Parker, *Soft Matter* **2012**, **8**, 6958-6967.
- [44] T. Feng, D. A. Hoagland, T. P. Russell, *Soft Matter* **2016**, **12**, 8701-8709.
- [45] Z. Zhang, Y. Jiang, C. Huang, Y. Chai, E. Goldfine, F. Liu, W. Feng, J. Forth, T. E. Williams, P. D. Ashby, T. P. Russell, *Science Advances* **2018**, **4**(8), 8045.
- [46] B. J. Kim, H. Kang, K. Char, K. Katsov, G. H. Fredrickson, E. J. Kramer, *Macromolecules* **2005**, **38**, 6106-6114.
- [47] J. Zhu, R. C. Hayward, *Angew Chem Int Edit* **2008**, **47**, 2113-2116.
- [48] J. T. Zhu, R. C. Hayward, *J Am Chem Soc* **2008**, **130**, 7496-7502.
- [49] R. J. Hickey, A. S. Haynes, J. M. Kikkawa, S. J. Park, *J Am Chem Soc* **2011**, **133**, 1517-1525.
- [50] Y. Q. Wu, K. Wang, H. Y. Tan, J. P. Xu, J. T. Zhu, *Langmuir* **2017**, **33**, 9889-9896.
- [51] K. H. Ku, J. M. Shin, D. Klinger, S. G. Jang, R. C. Hayward, C. J. Hawker, B. J. Kim, *ACS Nano* **2016**, **10**, 5243-5251.
- [52] A. Imhof, D. J. Pine, *Nature* **1997**, **389**, 948-951.

